RSC Advances

ROYAL SOCIETY OF CHEMISTRY

www.rsc.org/advances

RSC Advances

ARTICLE

Received 00th January 20xx,

Accepted 00th January 20xx

DOI: 10.1039/x0xx00000x

www.rsc.org/

Sputtering and sulfurization- combined synthesis of transparent WS_2 counter electrode and its application to dye-sensitized solar cells

Sajjad Hussain[a,b], Shoyebmohamad F. Shaikh[c,d], Dhanasekaran Vikraman[a,b], Rajaram S. Mane[c,e], Oh-Shim Joo[c,d], Mu. Naushad,[e] and Jongwan Jung[a,b,*]

In this work, continuous and large-area tungsten sulfide films, deposited by radio frequency sputtering followed by sulfurization process, were applied as a low-cost platinum-free counter electrode (CE) for dye-sensitized solar cell (DSCC). The composition and structure of WS_2 films were confirmed using X-ray diffraction, field-emission scanning electron microscopy, Raman spectroscopy and X-ray photoemission spectroscopy techniques. The WS_2 CE was phase pure and considerably transparent. The cyclic voltammetry, electrochemical impedance spectroscopy and Tafel curve showed that the WS_2 CE possesses high electrocatalytic activity and fast reaction kinetics for the reduction of tri-iodide to iodide, which can be attributed to its inherent catalytic property. Finally, TiO_2-based DSCC with an optimized WS_2 CE (sputtered for 10 min) showed as high as 6.3% power conversion efficiency, which is comparable to the performance of DSCC with platinum (Pt)-based CE (6.64%). Our study demonstrated the feasibility to develop low-cost, transparent, catalytically active, stable and abundant metal chalcogenide catalysts by RF sputtering method to replace Pt CE for photovoltaic application.

Introduction

The dye-sensitized solar cells (DSSCs) is a promising candidate for replacing traditional silicon-based solar cell due to its simple fabrication process, environmental friendliness, high power conversion efficiency (PCE), availability of an easy and low-cost sensitizers, simple production, high stability and wider range of design possibilities[1, 2]. To date, a myriad of efforts have been made to improve PCE of DSSCs by using platinum (Pt) counter electrode (CE), cobalt (II/III) electrolyte and zinc porphyrin[3]. Among them, conventional Pt as a CE is an expensive noble metal, which greatly restricts the commercial production of DSSC. Pt can also be decomposed to PtI_4 by $\frac{I^-}{I_3^-}$ redox couple in electrolyte[4, 5]. Many attempts have been made to replace the conventional Pt CE with low-cost alternatives such as graphite[6], carbon black[7], carbon nanotubes[8], conducting polymers[9], metal chalcogenides[10, 11], nitrides[12], carbides[13] and phosphides[14]. On the other hand, environmentally benign, abundant and non-expensive transition metal di-chalcogenides (MX_2, M = Mo, W and X = S, Se) have been the subject of extensive investigation due to their strong catalytic activities and potential applications[15-17]. Among the varieties of layered transition metal sulfides, tungsten sulfide (WS_2) is composed of three atomic layers: a tungsten layer is sandwiched between two sulfur layers, and the triple layers are stacked and held together by weak van der Waals interactions. It is an indirect band gap semiconductor with an energy gap of ~1.2 eV in bulk form[16, 18]. Due to its analogous structure to graphene and potential electrocatalytic activity, WS_2 has attracted great interest. WS_2 is extensively used for

[a]*Graphene Research Institute, Sejong University, Seoul 143-747, Republic of Korea*
[b]*Institute of Nano and Advanced Materials Engineering, Sejong University, Seoul 143-747, Republic of Korea*
[c]*Clean Energy Research Centre, Korea Institute of Science and Technology, Seoul, Republic of Korea*
[d]*School of Science, University of Science and Technology, 52 Eoeun dong, Yuseonggu, Daejeon 305-333, Republic of Korea*
[e]*Advanced Materials Research Chair, Department of Chemistry, College of Science, Bld-5, King Saud University, Riyadh, Saudi Arabia.*
* Corresponding author, E-mail: jwjung@sejong.ac.kr
Electronic Supplementary Information (ESI) available: [details of any supplementary information available should be included here]. See DOI: 10.1039/x0xx00000x

variety of applications such as solid state lubricants, catalysts for hydride sulfurization and hydrogen evolution reaction and anode materials for lithium ion batteries[19-21]. However, only a few reports have focused on the application of WS_2 as CE in DSSCs. Wu *et al.* [11]synthesized molybdenum sulphide (MoS_2) and WS_2 by a hydrothermal method. They employed them as CE materials for DSSCs and achieved PCEs of 7.59% and 7.73%, respectively. Recently, Yue *et al.* [22] reported DSCCs with a PCE of 6.41% under a simulated solar illumination of 100 $mWcm^{-2}$ (AM 1.5) using multi-wall carbon nanotubes decorated with WS_2 (MWCNTs-WS_2) CE, which were obtained using a hydrothermal method. However, to avoid the complex solution-based preparation process which is not eco-friendly, development of a pure WS_2 thin film directly grown onto a conductive substrate deserves further exploration. In this study, we present a scalable and reproducible RF sputtering method for the fabrication of a large area, continuous WS_2 film onto fluorine-tin-oxide (FTO)/glass substrate. The TiO_2-based DSSCs with an optimized WS_2 CE exhibited an impressive 6.3% PCE, which is comparable to DSSCs results with a Pt CE (6.64%).

Experimental Detail and Device Fabrication

Pieces of FTO/glass substrates (~ 2×2 cm^2) were ultrasonically degreased in acetone, methanol, isopropyl alcohol and deionized water and then baked at 120°C for 5 min. After loading the pieces in a sputter chamber, the chamber was evacuated by a rotary pump and a turbomolecular pump combination to achieve the pressure at ~ 1×10^{-7} torr. Next, WO_3 thin films were deposited onto FTO/glass substrates using a W target by RF magnetron sputtering. During the film deposition, the Ar and O_2 flow ratio was maintained at 5 and 15 sccm, respectively and the RF power was fixed at 180 W. The substrate temperature was fixed at room temperature. The sputtering time was varied (5, 10, 15 min) to control the thickness of WS_2 film. After taking out the samples from the sputter chamber, the as-sputtered films were placed downstream of a chemical vapor deposition (CVD) chamber and heated. The as-sputtered films were subjected to sulfurization process at 650°C for 30 min to form WS_2 film and also to improve the crystalline quality of the films. A pure sulfur powder (99.99%) was placed upstream of the CVD chamber, and a heating filament for the sulfur boat was fixed at 120°C. The sulfur powder was evaporated at 120°C using a carrier gas, Ar (100 sccm), and the pressure of the CVD chamber was kept at 2×10^{-2} mTorr. The distance between the sulfur boat and the substrate and the flow of the carrier gas were fixed for all the experiments. The amount of the sulfur powder was optimized at 0.5~0.8 g for the controlled growth of WS_2 film.

2.2 Fabrication of DSSCs using Pt CEs

A Pt CE was prepared by using a drop-cast method, as reported previously[23, 24]. In brief, a thin TiO_2 blocking layer with 100 nm thickness was deposited onto a FTO/glass substrate. A 0.2 M $TiCl_4$ (20–30 wt. % in HCl) was prepared using H_2O_2 at 50–55°C and crystallized at 350 °C for 60 min. After preparation of the solution, a few drops were placed onto the FTO/glass substrate and put on a hot plate at 70°C for 45 min. A TiO_2 layer (thickness ~ 4 μm) with an average particle size of ~20 nm was coated by the doctor blade method. A light scattering TiO_2 layer (thickness ~ 3 μm) was applied over the previously deposited TiO_2 and sintered again at 450°C for 30 min. The prepared TiO_2 photoanode was dipped in 0.3 mM N719 (ethanol + acetonitrile) dye for 24 hr so as to form working electrode for DSSCs. The DSSCs were fabricated by injecting a liquid electrolyte (0.005 M I_2, 0.1 M LiI, 0.6 M tetrabutylammonium iodide, and 0.5 M 4-tert-butylpyridine in acetonitrile) through an aperture between the dye-sensitized TiO_2 electrode and the CE (MoS_2 & Pt CEs, individually).

2.3 Characterization techniques

The phase purity analysis and structure confirmation of WS_2 CEs were studied using a Raman Microscope at 514 nm wavelength. The structural formation and crystal orientation were verified by using X-ray diffraction (XRD, Rigaku) with Cu-Kα radiation operated at 50 KV and 300 mA. The morphological evolutions of WS_2 films as a function of RF sputtering time were confirmed from the field-emission scanning electron microscopy (FE-SEM, Nova nano SEM200-100 FEI) images. Chemical configurations were determined by X-ray photoelectron spectroscopy (XPS), model PHI 5000 Versa Probe (Ulvac-PHI) using a monochromatic A_l K_α X-ray source (1486.6 eV). The data were collected from a spot-size of 100 x 100 μm^2. The carbon 1s peak (284.6 eV) was used as a reference for internal calibration.

2.4 Photo-electrochemical Measurements

A solar simulator (150 W Xe lamp, Sun 2000 solar simulator, ABET 5 Technologies, USA) equipped with an AM 1.5G filter was used to generate simulated sunlight with a corrected intensity of 1 sun (100 $mWcm^{-2}$). The photocurrent density-applied

voltage (*J-V*) spectra were obtained using a Keithley 2400 source meter. Incident photon current conversion efficiency (IPCE) spectra were obtained without bias potential under illumination with respect to a calibrated Melles-Friot silicon diode, and by changing the excitation wavelength (McScience K3100 spectral IPCE measurement system and Polaronix® K102 signal amplifier). Electrochemical impedance spectroscope (EIS) analysis was performed by IviumStat Technologies, Netherlands. The frequency of applied sinusoidal AC voltage signal varied from 150 kHz to 0.1 MHz.

Results and discussion

The schematic diagram of the WS_2 RF sputtering preparation process and DSSCs module is illustrated in **Figure 1**.

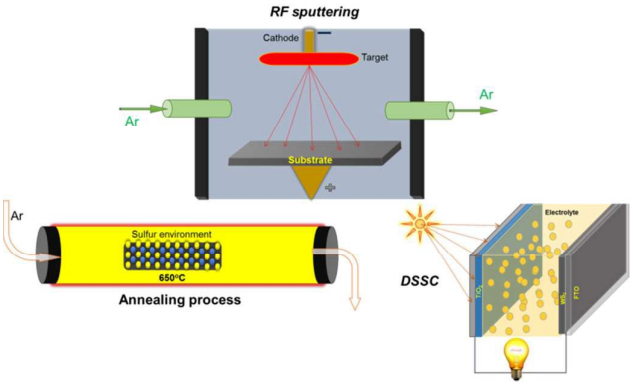

Fig. 1 Schematic diagram for preparation of WS_2 CE and its role in DSSCs.

Figure 2 (a-c) shows optical microscopy images of WS_2 films obtained at different sputtering time. The observed films seem to be uniform and continuous. Additionally, the films become darker (thicker) with increasing the sputtering time. Also, 3D images of prepared WS_2 films for different sputtering time are presented in **Figure (S1)**.

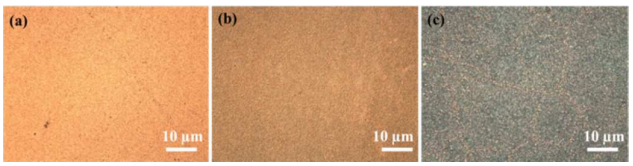

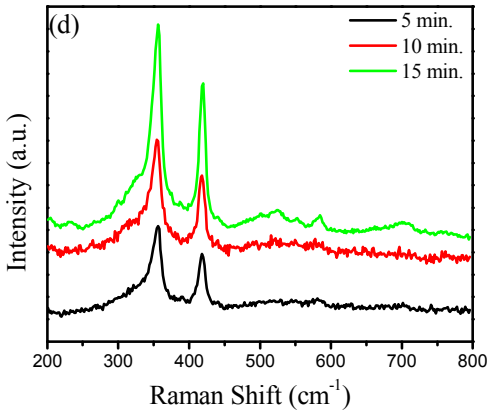

Fig. 2 (a-c) Optical images of WS_2 films obtained at different sputtering time; (a) 5, (b) 10 and (c) 15 min and (d) the Raman spectra of the corresponding WS_2 films (sputter time 5, 10 and 15 min).

Raman analysis was performed to perceive the crystal quality of WS_2. Raman spectra of the annealed WS_2 thin films are shown in **Figure 2(d)**. From **Figure 2(d)**, two characteristic WS_2 Raman peaks related to the in-plane vibration of W and sulfur atoms, E^1_{2g} mode at ~354.01 cm^{-1} and out-of-plane vibration of sulfur atoms, A_{1g} mode at ~418.4 cm^{-1}, were obtained. The frequency difference (Δk) between two Raman peaks is known to be closely related with the layer number and can be used to determine the thickness of atomically thin WS_2[25, 26]. The Δk increases with increasing sputtering time. The observed Δk is ~ 64.3 cm^{-1}, ~65 cm^{-1} and ~65.5 cm^{-1} for 5 min, 10 min and 15 min sputter time, respectively, corresponding to few-layer WS_2 films. [**Figure 2(d)**].

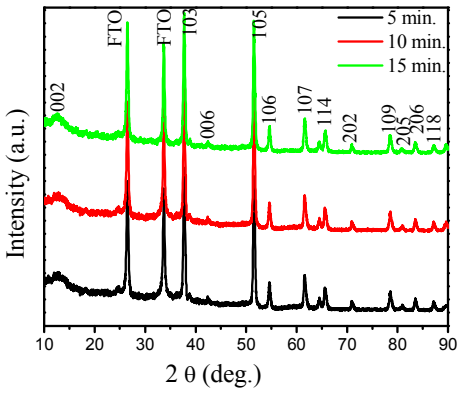

Fig. 3. XRD patterns of WS_2 films sputtered at different sputtering time of periods.

The crystallinity and purity of the WS_2 thin films were analysed by XRD analysis. From the **Figure 3,** all the reflections

were corresponding solely to WS_2 and substrate. The diffraction pattern revealed intense peaks at the positions of 37.2°, 42.9°, 51.1°, 54.6°, 61.6°, 65.7°, 70.9°, 78.3°, 80.5°, 83.5° and 87.5°, which were assigned to (103), (006), (105), (106), (107), (114), (202), (109), (205), (206) and (118) lattice planes of WS_2 crystal structure, respectively, evidencing that there was no trace of WO_3 after sulfurization process. The substrate-related FTO peaks were clearly emphasized in the XRD patterns. Presence of intense XRD peaks was an indication of the polycrystalline nature and the resultant diffraction peaks corroborate well with the standard patterns for the hexagonal crystal structure of WS_2 (JCPDS # 87-2417 file). The XRD results demonstrated no other phase transformation or other impurities in the crystalline film. The observed XRD reflections were highly sharp, indicating the high crystallinity of the WS_2 film surface. No other significant variations were observed in the XRD patterns for WS_2 films prepared at different sputtering time periods.

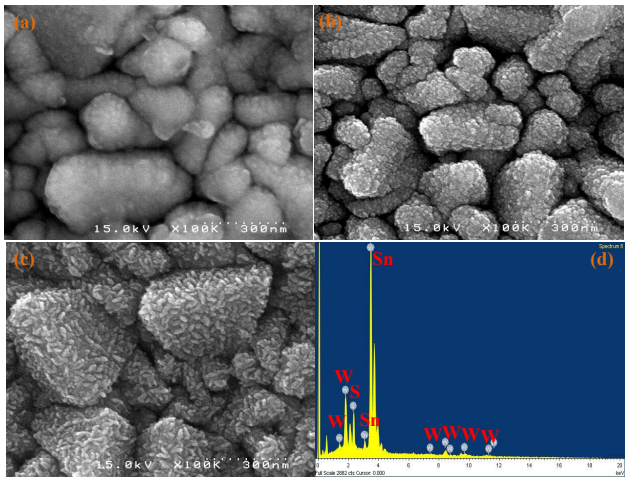

Fig. 4 FE-SEM micrographs of WS_2 CE sputtered for; (a) 5, (b) 10, and (c) 15 min. Elemental mapping of WS_2 (d).

Surface morphology acts as a key role in the development of thin film solar cells [27]. FE-SEM was used to see the surface morphology of the WS_2 material over FTO/glass substrate [Figure 4(a-c)]. Some crystallites larger than the normal due to the agglomeration process were detected. The valleys and hillocks were noticed over the sample prepared at 5 min-sputtering time [Fig. 4 (a)]. The various sizes and shapes of crystallites were noticed for WS_2 sputtered for 10 min [Fig. 4 (b)]. The highest crystallite sizes were found for WS_2 film sputtered for 15 min (Fig. 4c). The elemental mapping graph of WS_2 (Figure 4d) confirms the presence of Sn (from substrate), tungsten, and sulfur, which is consistent with XPS results mentioned below.

To further study the chemical composition and surface electronic states of WS_2, XPS analysis was carried out (sample sputtered for 10 min). The survey XPS spectra (Figure.5a) indicate the presence of sulfur, carbon, and oxygen etc., elements in the WS_2 film. The C_{1s} peak, related to sp_3 hybridized carbon, was observed at 284.8 eV [Figure 5b]. Figure (5c-d) shows the XPS spectrum of WS_2 film. The W 4f core-level spectrum showed three peaks corresponding to the W $4f_{5/2}$ and W $4f_{7/2}$ levels for W^{4+} and W $5p_{3/2}$ electronic state at 34.8, 32.7, and 38.0 eV, respectively. The S 2p core-level spectrum exhibited two peaks at 163.5 and 162.3 eV, corresponding to the S $2p_{1/2}$ and S $2p_{3/2}$ states, respectively. These results are well-consistent with the reported values for WS_2 single crystals.

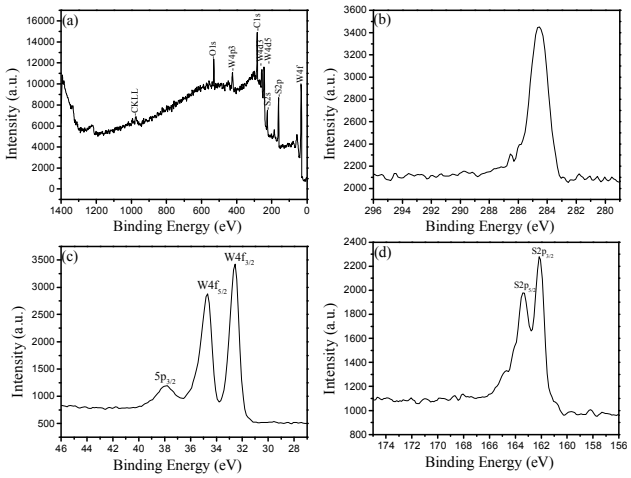

Fig. 5 XPS spectra of WS_2 film sputtered at 10 min; (a) Survey spectra, (b) carbon related C_{1S} peak, (c) tungsten doublet peak (W^{4+}), and (d) sulphur (S^{2-}).

In this study, the fabricated transparent WS_2 CEs were applied for DSSCs (Fig. 1). Figure S2 shows J–V characteristic curves of DSSCs with WS_2 CEs with different thickness. The obtained photovoltaic performance parameters are summarized in Table S1. The observed PCEs (η) of TiO_2-based DSSCs with WS_2 CEs sputtered for 5, 10 and 15 min were 5.4%, 6.3% and 5.8%, respectively. The highest efficiency was obtained from WS_2 CE sputtered at 10 min. J Wu *et al.*[28] demonstrated DSSCs with WS_2 CE, but the PCE of DSSCs based on pristine WS_2 CE was 5.32%. The PCE could be enhanced by inclusion of high-conductive MWCNT along with WS_2 in the presence of glucose so called as G-A WS_2/MWCNT hybrid CE. The PCE of our WS_2-based electrode are also superior to that of the previously reported plastic and carbon-coated WS_2 CEs[29].

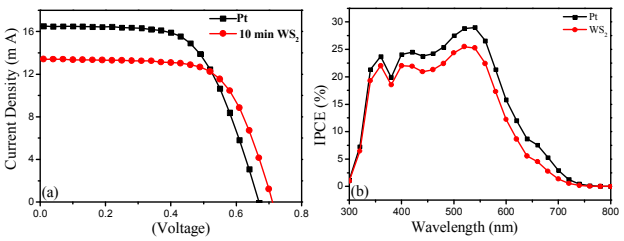

Fig 6. (a) J–V characteristic curves, (b) IPCE measurements of TiO_2-based DSSCs with WS_2 and Pt CEs.

Fig. 6a presents J–V characteristic curves of DSSCs with Pt and WS_2 CEs under illumination of 100 $mWcm^{-2}$. J-V curves of two DSSCs are nearly rectangular and identical, which demonstrates an excellent catalytic behaviour of WS_2 as like Pt. DSSCs employing WS_2 CE exhibits PCE of 6.3%, short-circuit current (J_{sc}) of 13.43 $mAcm^{-2}$, open-circuit voltage (V_{oc}) of 0.71 V, and fill factor (ff) of 0.66 [**Table 1**]. The IPCE curves of TiO_2-based DSSCs with Pt and WS_2 CEs (Fig. 6b) also present a similar behavior, suggesting that almost similar (to Pt) catalytic activity is obtained by the transparent WS_2 CE.

Table 1: DSSCs parameters of WS_2 (sputtered at 10 min) and Pt-CEs

	DSSCs type	J_{sc} (mA/cm^2)	V_{oc} (V)	FF (%)	η (%)
1	TiO_2-Pt CE	16.50	0.66	0.61	6.64
2	TiO_2-WS_2 CE	13.43	0.71	0.66	6.3

The PCE value for WS_2 CE is close to that obtained for DSSCs having a Pt CE (6.64%). The slight difference in the V_{oc} and J_{sc} values for the DSSCs with Pt and WS_2 CE can be attributed to several factors i.e., a) surface roughness difference, b) conductivity, c) catalytic activity, and d) chemical stability etc. Electrocatalytic activity is highly dependent on catalyst morphology, grain size, surface texture, crystalline structure and electrical conductivity of CE[30, 31]. The PCE dependence in DSSCs with different WS_2 film thickness (sputter time) can be attributed to the different morphology of the film with respect to the sputter time (Fig.4). The catalytic activity of WS_2 originates from the sulfur edges as reported previously. It is believed that with increasing the sputtered time more active sulfur edges are formed with increasing thickness and enhances the electro-catalytic activity [30,31].

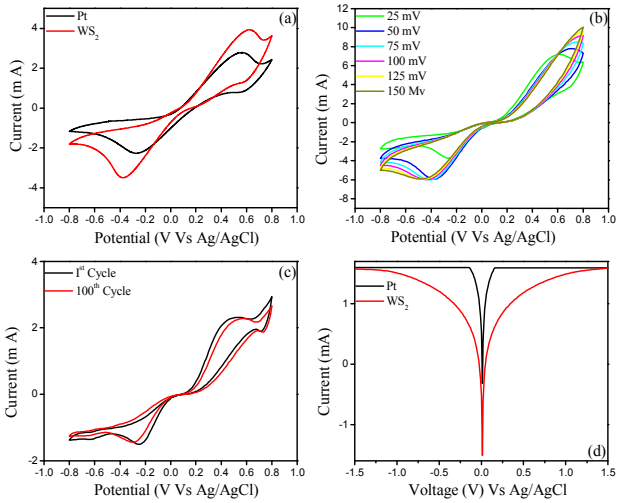

Fig 7. Cyclic voltammetry of; (a) I^-/I_3^- redox system using Pt and WS_2 CEs, (b, c) WS_2 CE at different scan rates and durability test for 100 consecutive cycles at a 10 mV s^{-1} scan rate. (d) Tafel polarization curves of symmetrical cells obtained with Pt and WS_2 CEs.

In this work, transparent (few-layer) WS_2 electrode was used for the first time as the CE material in DSSCs. To estimate the electrocatalytic performance of the WS_2 towards oxidation and reduction, cyclic voltammetry (CV) studies were performed. **Figure 7a** shows the CVs of the system for Pt and WS_2 in the potential interval between -0.8 to and 0.8V. In this process, electrons are injected into photo-oxidized dye from I^- ions in the electrolyte [Eq. (1)], and the produced I_3^- ions are reduced on the counter electrode [Eq. (2)]. In this interval, the anodic peak is contributed by the reaction (1) in an anodic sweep and the cathodic peak is contributed by the reaction (2) in a cathodic sweep, respectively.

$$I_3^- + 2e^- \Leftrightarrow 3I^- \quad \text{.....(1)}$$

$$3I_2 + 2e^- \Leftrightarrow 2I_3^- \quad \text{.....(2)}$$

More CV tests of WS_2 CEs for the $\frac{I^-}{I_3^-}$ redox reaction were carried out by changing scan rates (25~150 mVs^{-1}) as shown in **Figure 7b**. It was observed that the peak current densities were gradually increased with the increasing the scan rate. Simultaneously, the diffusion coefficient D of Pt and WS_2 CE can be estimated from the Randles-Sevcik equation:

$$I_p = Kn^{\frac{3}{2}} AC(D)^{\frac{1}{2}} V^{\frac{1}{2}} \quad \text{.....(3)}$$

where I_p represents the peak current, K is the constant of 2.69×10^5, n is the number of electrons transferred in the redox event, A is the electrode area, C represents the bulk concentration of I_3^- species , D is the diffusion coefficient and V means the scan rate. The diffusion coefficient of I_3^- for the Pt (~7.56×10^{-5}) is larger than that

for the WS_2 CE (~4.98 × 10^{-5}), presumably arising from the high active surface area and surface roughness difference of both electrode.

To investigate the electrochemical stability of the WS_2 CE, 100 consecutive CV cycles were performed in the potential region from - 0.8 to 0.8 V *vs*. Ag/AgCl [**Figure 7c]**. After 100 consecutive scans, the CV shape of WS_2 was changed a little and the current densities of its redox peaks remained stable, suggesting that the WS_2 CE possesses the characteristics of reversible activity, excellent electrochemical, chemical stability and strong adhesiveness on the FTO glass substrate. TiO_2 was used as a dye material and plays an important role due to many advantages such as having the most efficient photoactivity, highest stability and a low cost[32, 33]. Two types of photochemical reaction occur on the TiO_2 surface when irradiated with ultraviolet light. One includes the photo-induced redox reactions of adsorbed substances, and the other is the photo-induced hydrophilic conversion of TiO_2 itself [32, 34].

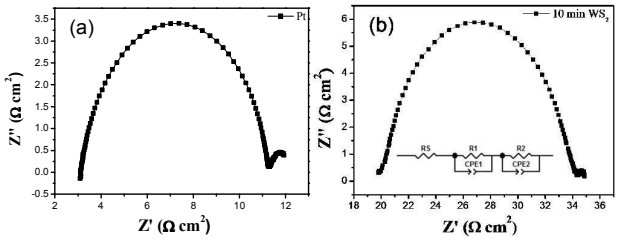

Fig 8. Nyquist plots for (a) Pt and (b) WS_2 CEs with inset of (b) as an equivalent circuit.

Tafel polarization measurements were performed on the symmetrical cells using WS_2 (10-min sputter time) and Pt CEs, and the corresponding curves are shown in **Figure 7d**. Also, Tafel polarization measurements of WS_2 obtained for different deposition time periods are given in **Figure (S4)**. The tangent slope of Tafel curves provides the information about the exchange current density (J_o). The commercial Pt electrode has larger J_o compared with sputtered WS_2 electrode, suggesting its higher electrocatalytic activity and lower charge-transfer resistance at the electrolyte–electrode interface.

Furthermore, EIS spectrums for symmetrical cells were carried out to examine the overall cell resistance. The Nyquist plots (Fig. 8a) for the symmetric cells with the Pt and WS_2 CEs illustrate impedance characteristics. The semicircle in the high frequency region (left) is due the charge-transfer process of the electrolyte-counter electrode interface, which changes inversely with the catalytic activity of the CE on the reduction of tri-iodide, and the corresponding constant phase element (CPE). The one in the low frequency region (right) is assigned to the Nernst diffusion process of tri-iodine ions. The impedance values (calculated using Z-View curve fitting software) are presented in Table 2. The R_{ct} value of the WS_2 and Pt CEs is 7.2 and 5.0 Ω cm^2, respectively. In addition, R_s is another important factor affecting the fill factor and performance of DSSCs [35]. Due to semiconducting behaviour, the WS_2 CE showed higher R_s value than Pt CE[36, 37]. Higher J_{sc} value in Pt CE DSSCs could be due to availability of its the large active surface area for $\frac{I^-}{I_3^-}$ redox reaction [38].

Table 2: EIS fitting parameters used for WS_2 and Pt CEs.

CE	Pt	WS_2
R_S (Ω cm^2)	3.1	19.5
R_1 (Ω cm^2)	8.11	13.39
$CPE_{1\text{-}t}$ ×10^{-3}	2.45	7.29
$CPE_{1\text{-}p}$	0.88	0.90
R_2 (Ω cm^2)	1.96	2.11
$CPE_{2\text{-}t}$ ×10^{-3}	0.98	0.50
$CPE_{2\text{-}p}$	0.60	0.096

Conclusion

In summary, continuous and large-area transparent WS_2 films deposited onto FTO substrate by RF magnetron sputtering were used as a low-cost and platinum-free counter electrode materials for dye-sensitized solar cells. X-ray diffraction and XPS have verified the phase purity and surface composition of WS_2 deposited onto FTO substrate. CV, EIS analysis and Tafel curve measurements indicated that the WS_2-based CE hold good electrocatalytic activity and fast reaction kinetics for the $\frac{I^-}{I_3^-}$ redox reaction. Finally, the DSSC with an optimized WS_2 CE (sputtered for 10 min) showed as high as 6.3 % PCE, which is comparable to the performance of DSCC with Pt CE (6.64 %). The present work demonstrated the feasibility to develop low-cost, transparent, efficient and abundant metal chalcogenide electrocatalysts (WS_2) with high catalytic activity and stability by RF sputtering method to replace Pt-based electrocatalysts for photovoltaic application.

Acknowledgements

This research was supported by the Basic Science Research Program through the National Research Foundation of Korea (NRF), funded by the Ministry of Education (2010-0020207, 2012R1A1A2007211), by the Human Resources Development of the Korea Institute of

Energy Technology Evaluation and Planning (KETEP) grant funded by the Korea government Ministry of Trade, industry & Energy (No. 20154030200630), and by the MOTIE(Ministry of Trade, Industry & Energy (10052928) and KSRC(Korea Semiconductor Research Consortium) support program for the development of the future semiconductor device. Authors, RSM and MN extend their gratitude to the Visiting Professor (VP) Unit of King Saud University (KSU) for the financial support.

References

1. B. O'regan and M. Grätzel, *Nature*, 1991, **353**, 737-740.
2. E. Stathatos, P. Lianos, U. Lavrencic-Stangar and B. Orel, *Advanced Materials*, 2002, **14**, 354.
3. A. Yella, H.-W. Lee, H. N. Tsao, C. Yi, A. K. Chandiran, M. K. Nazeeruddin, E. W.-G. Diau, C.-Y. Yeh, S. M. Zakeeruddin and M. Grätzel, *Science*, 2011, **334**, 629-634.
4. E. Olsen, G. Hagen and S. E. Lindquist, *Solar energy materials and solar cells*, 2000, **63**, 267-273.
5. A. Kay and M. Grätzel, *Solar energy materials and solar cells*, 1996, **44**, 99-117.
6. M. J. Ju, J. C. Kim, H.-J. Choi, I. T. Choi, S. G. Kim, K. Lim, J. Ko, J.-J. Lee, I.-Y. Jeon and J.-B. Baek, *ACS nano*, 2013, **7**, 5243-5250.
7. H. Choi, H. Kim, S. Hwang, W. Choi and M. Jeon, *Solar energy materials and solar cells*, 2011, **95**, 323-325.
8. T. Chen, L. Qiu, Z. Cai, F. Gong, Z. Yang, Z. Wang and H. Peng, *Nano letters*, 2012, **12**, 2568-2572.
9. L. Kavan, J.-H. Yum and M. Grätzel, *Nano letters*, 2011, **11**, 5501-5506.
10. C.-T. Li, C.-P. Lee, Y.-Y. Li, M.-H. Yeh and K.-C. Ho, *Journal of Materials Chemistry A*, 2013, **1**, 14888-14896.
11. M. Wu, Y. Wang, X. Lin, N. Yu, L. Wang, L. Wang, A. Hagfeldt and T. Ma, *Physical Chemistry Chemical Physics*, 2011, **13**, 19298-19301.
12. G. r. Li, F. Wang, Q. w. Jiang, X. p. Gao and P. w. Shen, *Angewandte Chemie International Edition*, 2010, **49**, 3653-3656.
13. A. Hauch and A. Georg, *Electrochimica Acta*, 2001, **46**, 3457-3466.
14. M. Wu, J. Bai, Y. Wang, A. Wang, X. Lin, L. Wang, Y. Shen, Z. Wang, A. Hagfeldt and T. Ma, *Journal of Materials Chemistry*, 2012, **22**, 11121-11127.
15. J. N. Coleman, M. Lotya, A. O'Neill, S. D. Bergin, P. J. King, U. Khan, K. Young, A. Gaucher, S. De and R. J. Smith, *Science*, 2011, **331**, 568-571.
16. Y. Zhang, Y. Zhang, Q. Ji, J. Ju, H. Yuan, J. Shi, T. Gao, D. Ma, M. Liu and Y. Chen, *ACS nano*, 2013, **7**, 8963-8971.
17. D. Voiry, H. Yamaguchi, J. Li, R. Silva, D. C. Alves, T. Fujita, M. Chen, T. Asefa, V. B. Shenoy and G. Eda, *Nat Mater*, 2013, **12**, 850-855.
18. A. L. Elías, N. Perea-López, A. Castro-Beltrán, A. Berkdemir, R. Lv, S. Feng, A. D. Long, T. Hayashi, Y. A. Kim and M. Endo, *ACS nano*, 2013, **7**, 5235-5242.
19. R. Bhandavat, L. David and G. Singh, *The Journal of Physical Chemistry Letters*, 2012, **3**, 1523-1530.
20. A. Sobczynski, A. Yildiz, A. J. Bard, A. Campion, M. A. Fox, T. Mallouk, S. E. Webber and J. M. White, *The Journal of Physical Chemistry*, 1988, **92**, 2311-2315.
21. L. Rapoport, Y. Bilik, Y. Feldman, M. Homyonfer, S. Cohen and R. Tenne, *Nature*, 1997, **387**, 791-793.
22. G. Yue, J. Wu, J.-Y. Lin, Y. Xiao, S.-Y. Tai, J. Lin, M. Huang and Z. Lan, *Carbon*, 2013, **55**, 1-9.
23. S. B. Ambade, R. B. Ambade, R. S. Mane, G.-W. Lee, S. F. Shaikh, S. A. Patil, O.-S. Joo, S.-H. Han and S.-H. Lee, *Chemical Communications*, 2013, **49**, 2921-2923.
24. X. Xin, M. He, W. Han, J. Jung and Z. Lin, *Angewandte Chemie International Edition*, 2011, **50**, 11739-11742.
25. H. Li, Q. Zhang, C. C. R. Yap, B. K. Tay, T. H. T. Edwin, A. Olivier and D. Baillargeat, *Advanced Functional Materials*, 2012, **22**, 1385-1390.
26. C. Lee, H. Yan, L. E. Brus, T. F. Heinz, J. Hone and S. Ryu, *ACS nano*, 2010, **4**, 2695-2700.
27. G. Yue, J.-Y. Lin, S.-Y. Tai, Y. Xiao and J. Wu, *Electrochimica Acta*, 2012, **85**, 162-168.
28. J. Wu, G. Yue, Y. Xiao, M. Huang, J. Lin, L. Fan, Z. Lan and J.-Y. Lin, *ACS applied materials & interfaces*, 2012, **4**, 6530-6536.
29. Y. Wang, S. Li, Y. Bai, Z. Chen, Q. Jiang, T. Li and W. Zhang, *Electrochimica Acta*, 2013, **114**, 30-34.
30. B. Hinnemann, P. G. Moses, J. Bonde, K. P. Jørgensen, J. H. Nielsen, S. Horch, I. Chorkendorff and J. K. Nørskov, *Journal of the American Chemical Society*, 2005, **127**, 5308-5309.
31. T. F. Jaramillo, K. P. Jørgensen, J. Bonde, J. H. Nielsen, S. Horch and I. Chorkendorff, *Science*, 2007, **317**, 100-102.
32. M. Thomalla and H. Tributsch, *The Journal of Physical Chemistry B*, 2006, **110**, 12167-12171.
33. M. Shanmugam, T. Bansal, C. A. Durcan and B. Yu, *Applied Physics Letters*, 2012, **100**, 153901.
34. N. G. Park and K. Kim, *physica status solidi (a)*, 2008, **205**, 1895-1904.
35. P. Joshi, L. Zhang, Q. Chen, D. Galipeau, H. Fong and Q. Qiao, *ACS applied materials & interfaces*, 2010, **2**, 3572-3577.
36. L. Han, N. Koide, Y. Chiba, A. Islam, R. Komiya, N. Fuke, A. Fukui and R. Yamanaka, *Applied Physics Letters*, 2005, **86**, 213501.
37. N. Koide, A. Islam, Y. Chiba and L. Han, *Journal of Photochemistry and Photobiology A: chemistry*, 2006, **182**, 296-305.
38. C. H. Yoon, R. Vittal, J. Lee, W.-S. Chae and K.-J. Kim, *Electrochimica Acta*, 2008, **53**, 2890-2896.